

1 Persistent Deformation in a Post-Collisional Stable 2 Continental Region: Insights from 20 Years of cGPS in 3 Romania

4 Alexandra Muntean^{1*}, Laura Petrescu^{1,2}, Boudewijn Ambrosius³, Felix Borleanu¹, Eduard Ilie
5 Nastase¹, Ioan Munteanu^{4,5}

6 1. National Institute for Earth Physics, Magurele, 077125, Romania

7 2. Faculty of Physics, University of Bucharest, Magurele, 077125, Romania

8 3. Faculty of Aerospace Engineering, Delft University of Technology, Delft, 2629HS, The Netherlands

9 4. Faculty of Geology and Geophysics, University of Bucharest, Bucharest, 010041, Romania

10 5. Romanian Academy Institute for Geodynamics “Sabba Stefanescu”, Bucharest, 020032, Romania

11 *Correspondence to:* Alexandra Muntean (muntean@infp.ro), Laura Petrescu (laura.petrescu@infp.ro),

12 Boudewijn Ambrosius (bacambrosius@gmail.com).

13 **Abstract.** The Carpathian Region, located at the edge of the East European Platform, presents a unique tectonic
14 setting where major deformation associated with subduction and collision appears to have ceased around 8 million
15 years ago. Yet vertical movements and present-day seismicity continued afterward, suggesting ongoing crustal
16 deformation and challenging our understanding of intraplate earthquakes and the processes driving these
17 phenomena in an area considered a stable continental interior. In this study, we analyze over two decades of
18 continuous GPS (cGPS) data from 143 permanent stations to estimate both horizontal and vertical crustal motions,
19 constructing the most accurate model of crustal deformation in the region to date. The estimated velocity field
20 indicates a southward drift of the South Carpathians and Moesia relative to Eurasia, with velocities ranging from
21 0.5 to 2 mm/yr. We detect a more complex pattern of vertical uplift and subsidence in the foredeep, challenging
22 a previously held view that this region is solely subsiding. This pattern may reflect localized uplift in response to
23 processes such as the Vrancea Slab break-off beneath the South-East Carpathians. Crustal scale active faults
24 accommodate the observed differential motion, fragmenting the foreland. Furthermore, using a regularized
25 horizontal velocity vector field, we estimate strain rate variations, maximum shear strain, and dilatation patterns
26 across Romania, that align with observed stress regimes and earthquake mechanisms. This agreement validates
27 our results and indicates an influence of surface plate kinematics on the observed seismicity, in addition to the
28 deep Vrancea Slab dynamics. Our findings provide insights into the causes of crustal deformation at the transition
29 between active collision zones and stable continental platforms, enhancing our understanding of intraplate
30 seismicity in regions traditionally considered tectonically stable.

31 **Keywords:** deformation, GPS, crustal motion, geology, tectonics

32 1. Introduction

33 A key tectonic question lies in understanding the nature of active deformation and frequent seismicity in regions
34 situated at the transition between active subduction/collision systems and more stable continental interiors. The
35 Carpathian Region in Romania marks such a transition between the active Africa-Eurasia subduction system to

36 the south and the stable continental core of Eurasia: the East European Platform (Fig. 1). Although this area is not
37 considered a traditionally active plate boundary, with most geological evidence suggesting that major deformation
38 associated with the collision ceased around 8 million years ago (Maţenco and Bertotti, 2000), it continues to
39 experience frequent crustal and subcrustal seismicity. Active deformation and seismicity are observed along major
40 faults and geological contacts (e.g., swarms near Tg. Jiu and Galaţi, Craiu et al., 2017; Radulian et al., 2023;
41 Borleanu et al., 2024). Notably, the Vrancea Slab, a relic lithospheric plate sinking, retreating and stretching
42 beneath the East Carpathians Bend Zone, may still be coupled with the overlying crust, as suggested by the
43 thermochronological studies, which showed an increase in uplift, post 8 Ma, especially along the western flank
44 of the Focsani Basin (Necea et al., 2005, 2013, 2021). This coupling could be driving long-term surface
45 deformation (Ismail-Zadeh, 2012; Petrescu et al., 2021), contributing to ongoing seismicity (Radulian et al., 2019;
46 Petrescu et al., 2025) and exhibiting the largest present-day strain concentration in continental Europe (Wenzel et
47 al., 1999).

48 Measuring crustal motion is relevant for understanding ongoing deformation processes and seismic hazards in
49 such a tectonically complex region. In this study, we estimate both horizontal and vertical motions using Global
50 Positioning System (GPS) data from permanent stations that operated in Romania in the past 20 years. These
51 measurements provide key information about how the region is deforming and how this relates to the observed
52 seismicity. The data also shed light on the connection between surface deformation and subsurface dynamics,
53 including the potential role of the sinking slab in driving seismic activity. Furthermore, the GPS data allows us to
54 assess whether deformation is concentrated along major fault zones or more broadly distributed across the crust,
55 offering a clearer picture of how past tectonic events continue to shape the region's seismic behavior.

56 The first vertical velocity maps of Romania, based on repeated leveling data from first- and second-order national
57 network lines, were published by Cornea et al. 1978, 1979a 1979b. Following the major earthquake of March 4,
58 1977 (M7.2), high-accuracy leveling measurements allowed for the development of a more refined vertical
59 velocity map (Popescu and Dragoescu, 1987). Subsequent research extended these efforts to the broader Carpatho-
60 Balkan region (Joo et al., 1987). Dinter and Schmitt (2001), after two years of GPS monitoring in Romania,
61 detected no measurable deformation but recommended expanding the network and conducting repeated
62 measurements at two-year intervals to capture crustal dynamics better. Van der Hoeven et al. (2005) later
63 published results from annual GPS campaigns conducted between 1997 and 2004. However, velocity solutions
64 derived from temporary GPS deployments were subject to influences such as equipment changes, monument
65 removals, and antenna setup inconsistencies, as well as local effects such as sediment compaction and site
66 instability. Compared to the high precision of modern continuous GPS (cGPS) solutions, the historical campaign
67 data exhibit 3 to 4 times higher uncertainty (van der Hoeven et al., 2005). These limitations highlight the need for
68 continuous GPS measurements to better resolve crustal and mantle dynamics in geologically active regions.

69

70

71

72 2. Tectonic setting

73 The tectonic evolution of the Romanian region is essential for understanding present-day deformation and seismic
74 activity. The Carpathian Mountains dominate the topography, with neo-tectonic and associated seismicity
75 pervasive in the East Carpathians Bend Zone and extending into the South Carpathians and the surrounding
76 foreland (Petrescu et al., 2021), underlain by the Moesian Platform (MP), a thick lithospheric block with
77 Precambrian-aged basement, shaped by multiple tectonic phases throughout the Paleozoic to Cenozoic times (Fig.
78 1). The MP is bounded by two Alpine Orogens, the Carpathians to the north and West and the Balkanides to the
79 south, while the eastern margin extends into the Black Sea Basin. It is largely covered by Neogene sediments and
80 extends eastward to the Black Sea, where its uplifted basement is exposed in the Dobrogea Region. The platform
81 is separated into crust blocks by several faults, such as the Intra-Moesian Fault (IMF) and the Capidava-Ovidiu
82 Fault (COF, Fig. 1).

83 To the northeast, the MP transitions into the East European Platform (EEP), a thick and geologically stable
84 continental core that forms part of the Eurasian Plate. The boundary between the two is marked by the North
85 Dobrogea Orogen (NDO) (Hippolyte, 2002), a remnant of the Hercynian Orogeny (Seghedi et al., 1999), located
86 between the Peceneaga-Camena Fault (PCF) and Sfântul Gheorghe Fault (SFG, Fig. 1). Part of this now partially
87 eroded orogen is buried beneath Neogene foredeep sediments from the younger Carpathian collision, while to the
88 east, it has undergone uplift.

89 Over the past 20 million years, the concomitant roll-back of the Carpathian and Dinaridic Slab Adria Plate, led to
90 the opening of the Pannonian Basin coeval with the formation of the Carpathian Fold and Thrust Belt and
91 associated foreland basin (Balla, 1986; Barrier et al., 2018; Maţenco and Radivojevic, 2012), essentially shaping
92 the present-day European continent (Schmidt et al., 2020). In Romania the slab roll-back forced the clock wise
93 rotation of the Carpathian Orogen and obliquely thrusting over the foreland units MP, forming the South
94 Carpathians, and collided with the passive margin of the East European Platform, creating an asymmetric
95 foreland basin (Sandulescu, 1984; Maţenco and Bertotti, 2000; Csontos and Vörös, 2004).

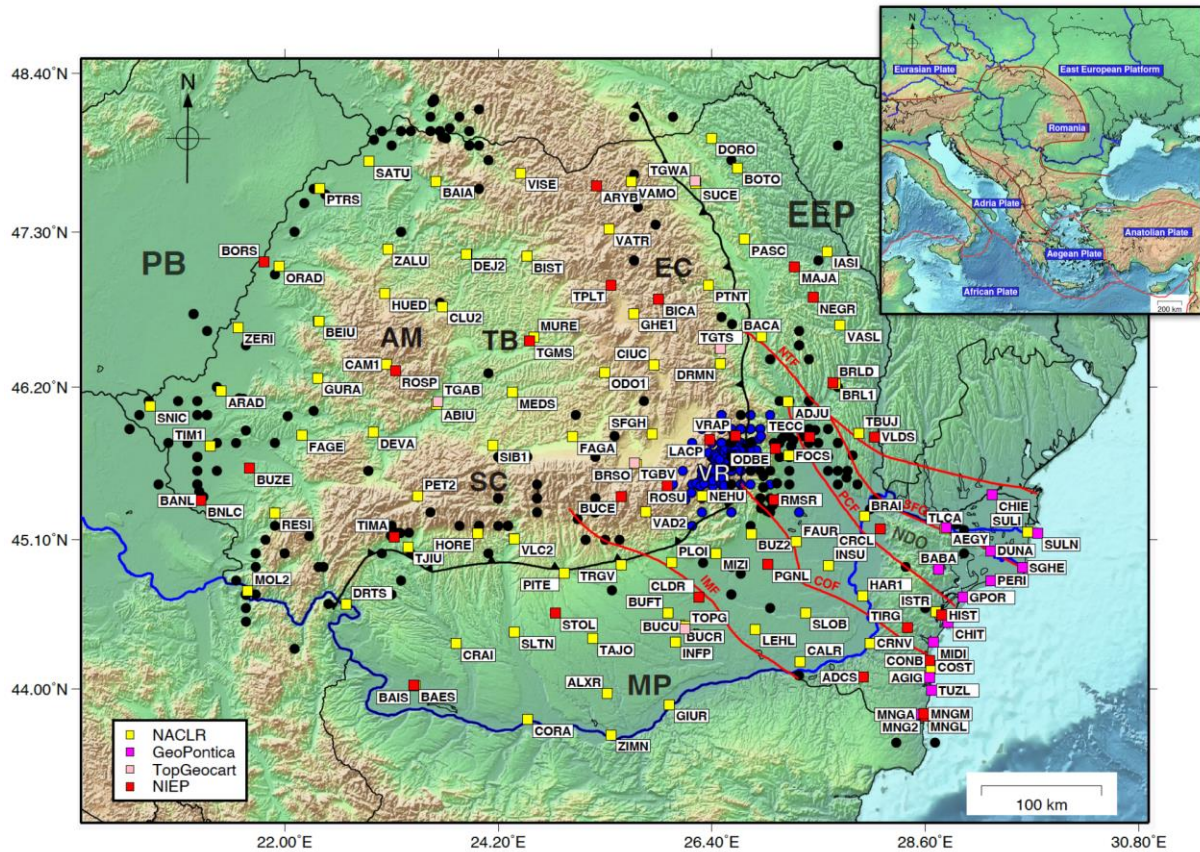
96 Beneath the Southeast Carpathians, where multiple tectonic units interact, the notorious Vrancea Slab, a
97 lithospheric block that is plunging almost vertically into the mantle (Ren et al., 2012). It is stretching and causing
98 frequent high-magnitude destructive earthquakes in Romania, both at intermediate depths and in the overlying
99 crust (Radulian et al., 2019; Petrescu et al., 2021; Enescu et al., 2023). Analysing the crustal motions above this
100 sinking slab provides an opportunity to gain insights into crustal deformation in a triple-junction tectonic setting
101 (Besutiu et al., 2017). Major collisional related shortening deformation in the Carpathians is thought to have ended
102 around 8-11 Ma, based on the cessation of late Miocene thrusting (Maţenco et al., 2007 and references therein),
103 while fission-track analysis suggests the onset of exhumation (or uplift) at 4 Ma in the SE Carpathians and 12 Ma
104 in the East and South Carpathians (Sanders et al., 1999; Cloetingh et al., 2006). Present-day GPS measurements
105 provide valuable insights into how these long-term geological processes continue to shape ongoing crustal motion
106 and deformation, particularly in the Vrancea Zone (Fig. 1), where active subduction and slab-related dynamics
107 are still influencing surface motion. The crustal deformations observed today are also influenced by the relative
108 motion of surrounding crustal blocks, complicating the understanding of the region's complex and dynamic
109 geological behavior.

110 3. Continuous GPS (cGPS) Networks in Romania

111 We analyzed data from cGPS stations across Romania, which are part of four different networks (Fig. 1). The
112 primary network, supported by the National Institute for Earth Physics (NIEP), was first developed in 2001.
113 Initially, the network consisted of seven stations, equipped with Leica CRS1000 receivers and LEIAT504 choke-
114 ring antenna protected by a dome. These stations were placed in remote areas and were designed to operate with
115 minimal maintenance, relying on power converters and batteries. Over time, the network has grown, and today it
116 includes 33 stations, with five of the original stations still in use. The newer stations are equipped with Leica
117 GRX1200, LEIAR GR30, and GR50 receivers. Most of the antennas are Leica (LEIAT504, LEIAR10, LEIAR20)
118 and are placed on concrete pillars. Only one is mounted on a polar mast (MNG2). The stations transmit real-time
119 data via the internet, and NIEP is responsible for the equipment, installation, ongoing maintenance, and data
120 analysis.

121 We also used GPS data from the GeoPontica network, developed by the National Research and Development
122 Institute for Marine Geology and Geoecology (GeoEcoMar), the National Center for Monitoring and Alarm to
123 Natural Marine Hazards – Euxinus, covering the period from 2013 to the present. This network includes 13
124 stations, the antennas are mounted on a deep-drilled, braced monument. In addition, we included data from the
125 ROMPOS (NACLAR) network, managed by the National Agency for Cadastral and Land Registration, comprising
126 86 reference stations across Romania. We were also granted access to data from the private TopGeocart network,
127 which includes 8 stations. Most of these GPS antennas are mounted on building rooftops or fixed to the structures
128 housing the receivers.

129 In total, this selection resulted in 143 available stations. The data are stored in a repository, organized by network,
130 year and Julian day, in the Receiver Independent Exchange (RINEX) version 2 and 3 format, sampled at 30s
131 intervals. For this study, we only selected stations that are (still) operational after January 01, 2024. This reduced
132 the selection to 130 stations(Fig.1).



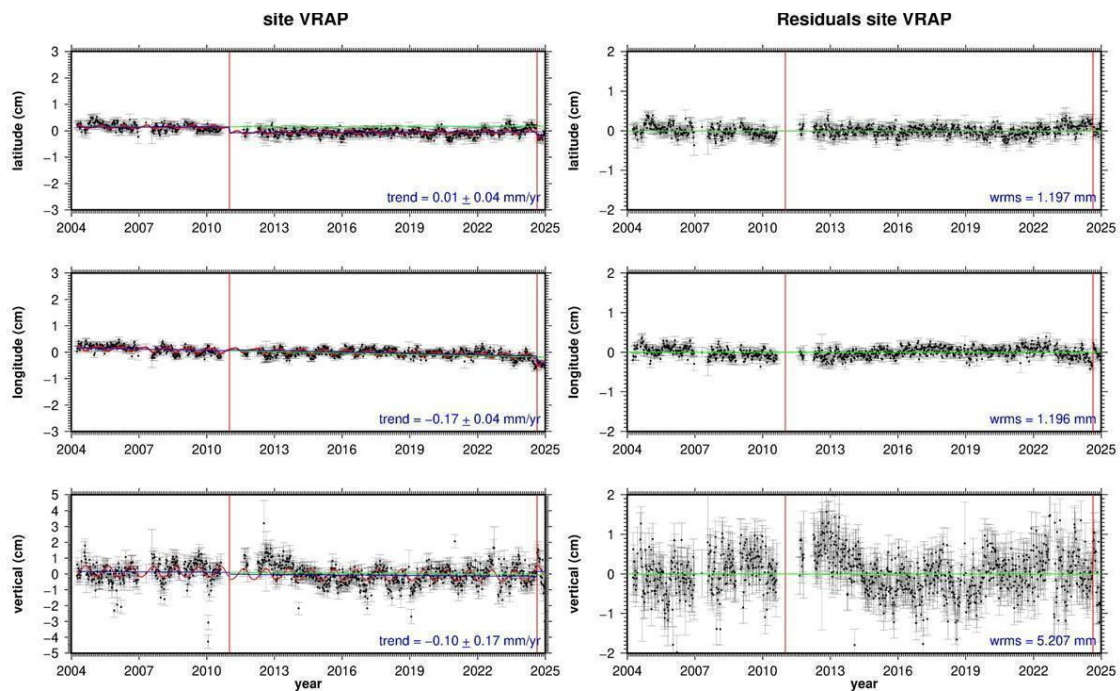
133
 134 **Figure 1: The distribution of the available cGPS stations used in this study (coloured squares), and earthquakes**
 135 **distribution according to the Romanian earthquakes catalog (ROMPLUS, Popa et al., 2022) between August 1679 and**
 136 **September 2024. Earthquakes are color-coded by depth: black for crustal events ($H < 60$ km, $M_w > 3.5$), blue for**
 137 **intermediate-depth events ($60 < H < 167$ km, $M_w > 4$). The major faults are plotted as solid red lines and identified**
 138 **with their acronyms in a blue box: IMF - Intra-Moesian Fault, COF - Capidava Ovidiu Fault, PCF - Peceneaga Camena**
 139 **Fault, NTF - New Trotuș Fault, and SFG - Sfântu Gheorghe Fault. The old trust fault is represented by a solid, black,**
 140 **toothed line. The major tectonic units are in bold characters: AM - Apuseni Mountains, SC - South Carpathians, EC -**
 141 **East Carpathians, VR – Vrancea, NDO - North Dobrogea Orogen, PB - Pannonian Basin, TB - Transylvanian Basin,**
 142 **EEP - East European Platform, and MP - Moesian Platform. Further acronyms in the color legend box include:**
 143 **NACLR - National Agency for Cadastre and Land Registration, GeoPontica - National Research-Development**
 144 **Institute for Marine Geology and Geoecology GNSS network, TopGeocart is a private company, operating its own**
 145 **GNSS network, NIEP - National Institute for Earth Physics. The inset shows the regional tectonic setting, with plate**
 146 **boundaries indicated in red.**

147 **4. GPS data processing**

148 For the data processing, we use the GipsyX software (Bertiger et al., 2020), developed at NASA's Jet Propulsion
 149 Laboratory (JPL), Pasadena, USA. It features Precise Point Positioning (PPP), which enables (daily) geodetic
 150 position determination of a single GPS station. Accuracy can vary depending on the quality of the GPS receiver,
 151 the antenna, and local conditions (e.g., multipath). Weekly updated data files, provided by JPL, contain precise
 152 GPS satellite orbits, Earth Rotation Parameters (ERP), satellite clock corrections, spacecraft altitude information,
 153 and so-called wide lane phase biases to enable signal ambiguity resolution. In addition, we apply ocean loading
 154 corrections for each station, obtained from the Onsala Space Observatory, Chalmers University of Technology
 155 (Bos and Scherneck, 2011). To model the wet tropospheric signal delays, we use data from VMF (Vienna Mapping
 156 Functions) (re3data.org:VMF Data Server).

157 Processing the recordings from the 130 selected stations with this software resulted in a repository with daily
 158 solutions for each station. Subsequently, to reduce noise, we combined the daily solutions into weekly ones. Then,
 159 we converted the reference plate of these solutions to the Eurasian tectonic reference plate using the ITRF14
 160 rotation parameters of that plate (Altamimi et al., 2017). From this data, we created a time series for each station.
 161 To evaluate the impact of reference frame choice, we tested several local transformation approaches, including
 162 Euler pole rotation, network mean removal, and selected-station mean removal. Statistical comparisons showed
 163 that the Euler pole rotation was similar to the EU14 reference frame which further justifies using EU14 as our
 164 preferred reference frame (Figs. S1, S2 and S3; Tables S5 and S6 in the Supplementary Material - SM).

165 Next, we estimated a linear trend (velocity) and yearly and half-yearly seasonal signals. In addition, for
 166 undocumented changes, the estimation model also includes position jumps at times identified from an inspection
 167 of the raw time series. All recent time series are affected by a reference frame change on August 19, 2024, by
 168 JPL. These are now also modeled as position jumps. An example of the results is presented in Figure 2 for the
 169 long-lived station VRAP. Apparently, this station was re-equipped in 2011, and from the vertical residuals, it
 170 seems that it took a few years to settle down on its original monument.



171
 172 **Figure 2: Time series of the VRAP station. The left panel shows the raw series with the modeled functions. The red**
 173 **curve represents the estimated yearly and half-yearly functions. In the left panel the green line represents the estimated**
 174 **velocity before the first jump. The vertical red lines represent position jumps. The right panel shows the residuals after**
 175 **subtracting the modeled functions, including the estimated position jumps.**

176 4.1 Horizontal time series selection and quality control

177 In this step, to ensure the best possible quality of the time series solutions, we selected stations with uncertainties
 178 (sigmas) less than 0.2 mm/yr and velocity vectors smaller than 2 mm/yr. We consider that these criteria guarantee
 179 a reliable selection of credible solutions. However, a small number of these sites still exhibit anomalous velocities.
 180 These are likely caused by local effects such as landslides, station instability, local geological conditions,
 181 subsurface compaction, undocumented antenna changes, and multipath interference. The main reason is that most
 182 GPS antennas are mounted on buildings and unstable steel rods. In our analysis, we try to model them as position

183 jumps. The dates of these “unknown” jumps were established using a manual process by examining the “raw”
184 time series plots for each station.

185 This process automatically eliminates the shorter lived time series, reducing the number of accepted solutions to
186 99, with the shortest series extending more than four years. This means that all 99 accepted solutions satisfy the
187 criterion established by Blewitt et al. (2001), who claim that the series should be longer than two and a half years
188 for a reliable estimate of the seasonal terms, which is essential for the reliability of the velocity estimate.

189 The accuracies (σ) at the 95% confidence level were estimated using the weighted root mean square (WRMS) of
190 the fit according to the formula:

$$191 \quad \sigma = \frac{2 \cdot WRMS}{2.4 \cdot T_{span}}$$

192 where T_{span} is the length of the time series in years. This approach provides estimates of velocities and their
193 uncertainties. This empirical approach relates the scatter of the residuals to the stability of the velocity estimate
194 and provides a practical measure of the combined effect of unmodeled noise sources. A similar approach has been
195 previously applied in geodetic studies (e.g., Muntean et al., 2016).

196 The use of WRMS-based uncertainties is justified by the relatively long duration of the analyzed time series (all
197 exceeding four years), which reduces the impact of temporally correlated noise on velocity estimation. In addition,
198 careful modeling of discontinuities (e.g., offsets due to equipment changes or local effects) further minimizes bias
199 in the residuals. Under these conditions, the adopted approach provides stable and internally consistent uncertainty
200 estimates across the network. Quantitatively, the mean uncertainty is 0.12 mm/yr, yielding a mean signal-to-noise
201 ratio of 4.9, with values reaching up to 15. These results indicate that the observed velocities significantly exceed
202 their formal uncertainties and are therefore well resolved (Fig. S4).

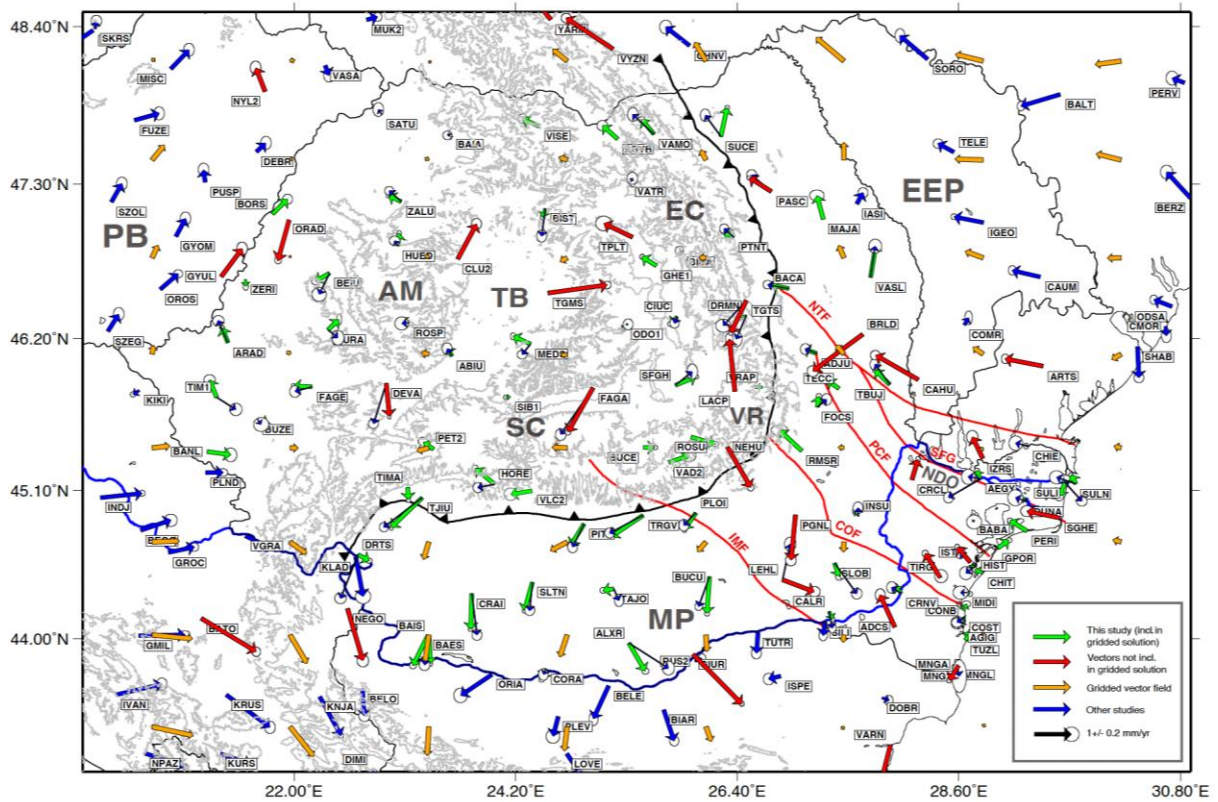
203 We also compared our results with those of Piña-Valdés (2022) for stations with common solutions and found an
204 average difference of less than 0.08 mm/yr (Fig. 3, and Figs. S4 and S5, SM). This level of agreement demonstrates
205 general consistency. The results for the 99 accepted sites are summarized in Table S1 in SM.

206 **4.2 Creating a gridded, smooth horizontal velocity field**

207 To create a smooth, coherent representation of the computed time series solutions, we use a spatial gridding
208 approach: we set up an 8 x 8 grid of latitude and longitude nodes with each node linked to a square search box.
209 The size of these boxes depends on the distance (in km) between nearby nodes, ensuring the north-south and east-
210 west dimensions are equal. the next step, we eliminate outliers with a velocity larger than two times the median.
211 Then, we calculate the average of the EW and NS velocity components of the remaining solutions. During this
212 process, 22 of the 99 solutions are excluded as outliers. The final result is a gridded dataset of 47 nodes showing
213 the velocities for each node. The other 17 nodes are not presented since there were no Romanian cGPS stations
214 available in the search area (see Table S2, SM).

215 When we include the literature (Piña-Valdés et al., 2022; Serpelloni et al., 2022), solutions for the countries
216 neighbouring Romania, the number of solutions increases to 160. After applying the aforementioned editing step,

217 this number decreases to 133. These solutions are based on a collection of shorter time series from before 2021.
 218 Nevertheless, they provide valuable additional information.



219
 220 **Figure 3: GPS-derived horizontal velocity vectors with respect to the ITRF-2014 Eurasian plate according to Altamimi**
 221 **et al. (2017). Green vectors represent our results, blue vectors were taken from Piña-Valdés et al. (2022). The red**
 222 **vectors were excluded while creating the interpolated velocity field on a regular (8 x 8) grid, represented as orange**
 223 **vectors. The error ellipses are 95% confidence level. Faults and acronyms are as in Figure 1.**

224 **4.3 Vertical data selection**

225 For the vertical component, we apply a different approach. This component is hardly affected by horizontal station
 226 instabilities, but mostly by undocumented antenna changes. We tackle this problem by estimating vertical position
 227 jumps on the dates when they appear in the time series. Furthermore, we select only solutions with an absolute
 228 velocity < 2 mm/yr and an accuracy < 1.0 mm/yr, which we consider credible. Some sites show subsidence, but
 229 these are mostly located in coastal areas, on slow landslides, and compacting sedimentary areas. As a result, from
 230 the 130 available solutions of the four Romanian permanent networks, 95 solutions were accepted (Fig. 4). The
 231 results are presented in Figure 4 and Table S3 (SM). We also compared our solutions with those of Piña-Valdés
 232 (2022), and found an average difference of less than 0.03 mm/yr.

233 When we include the literature solutions, the pattern does not change much. It mostly adds subsidence sites in the
 234 area west and south-west of Romania. The total number of accepted vertical sites increased to 145.

256 Carpathians, which are obliquely thrust over the MP, defined by strong and sometimes sharp lateral variation in
257 rheology across the major faults like IMF or COF, which imposed the formation of tear-faults and oblique ramps
258 into the Carpathian Orogen (Fig. 3). Hence, the magnitude and direction of motion vary significantly across the
259 IMF and COF or other major faults in the MP and foreland units in general, like PCF and NTF, that are defining
260 crustal blocks with different rheologies, thermal history, and response under the orogenic loading. In contrast,
261 vectors in the EEP show a slight northwestward motion relative to the Eurasian plate. This shift occurs across the
262 PCF and NTF, which define the boundaries of the North-Dobrogea Orogen (Fig. 3), a transitional zone between
263 the EEP margin and the MP. As a result, the EEP undergoes a subtle yet persistent movement relative to Eurasia,
264 diverging from the southward-moving MP through a series of crustal-scale faults that accommodate lateral
265 displacement.

266 The Transylvanian Basin (TB) and the East Carpathians, on the other hand, show minimal horizontal motion. GPS
267 stations in these areas indicate limited deformation, with inconsistent directional patterns and low overall
268 coherence in movement. Small horizontal motions are observed in the Pannonian Basin (PB) in an NNE direction,
269 which reoriented toward different directions near the Apuseni Mountains (see Figs. 1 and 3).

270 Overall, the foreland region, particularly the MP, appears to be drifting southward, while the other areas remain
271 relatively stable, indicating that the foreland is more dynamically active than the surrounding regions.

272 **5.2 The vertical velocity field**

273 The Carpathians predominantly experience uplift (Fig. 4), concentrated in the East Carpathians (e.g., BICA,
274 TPLT), and the South Carpathians (e.g., VAD2, and PITE). While some scattered stations (ROSU, TGTS) indicate
275 subsidence, the overall trend suggests uplift rates ranging between 0.5 and 2 mm/yr. The Vrancea bend zone is an
276 interesting exception because it only shows a minor uplift (e.g., LACP and VRAP).

277 The foreland region exhibits an intricate interplay of uplift and subsidence. The Moesian Platform, which occupies
278 the area bounded by the Carpathians, the Balkans and the Black Sea, shows a north-south dichotomy in vertical
279 motion. In its southern part, across the E-W trending Danube River and towards the Balkans, the crust is
280 predominantly subsiding. Northward and northeastward toward the Carpathians, the Capidava-Ovidiu Fault, the
281 trend gradually transitions to uplift. The most pronounced uplift occurs in Dobrogea, the exposed basement of the
282 Moesian Platform near the Black Sea, where all geodetic stations record consistent uplift along the coast and the
283 Danube. Notably, the Danube changes its course northward across this transition zone.

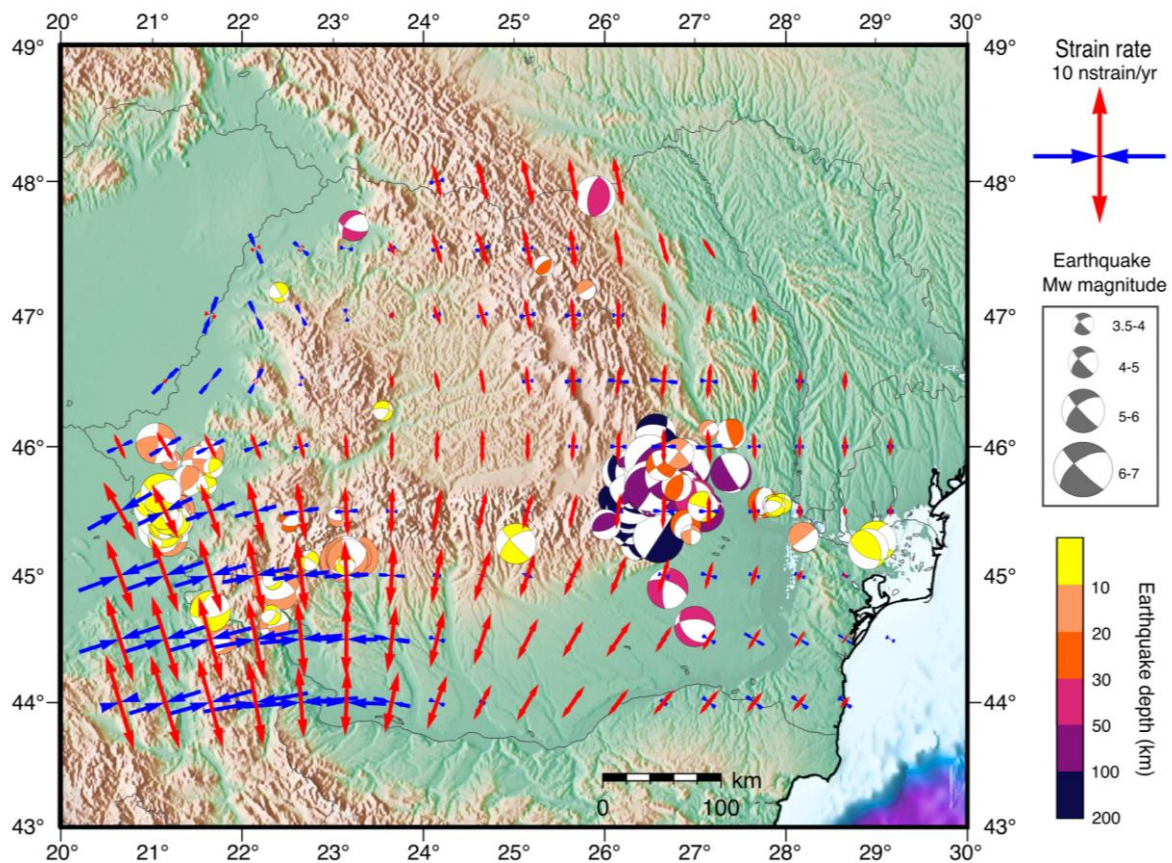
284 The East European Platform, forming the eastern foreland of the Carpathians, exhibits only minor vertical
285 movements. Several stations in its northern part record slight uplift, which transitions southward into subsidence
286 toward the Neogene Troțuș Fault known in literature as the New Troțuș Fault (Matenco et al, 2007). This subsiding
287 trend extends farther south into parts of the NDO continuing across the SFG and the PCF, which delineates the
288 boundary with the MP. On the opposite side, the MP is undergoing uplift, reflecting strong differential crustal
289 deformation along these seismically active fault networks.

290 In the backarc region relative to the Carpathians, in the Transylvanian and Pannonian basins, estimated crustal
291 motions suggest subsidence relative to stable Eurasia. However, the Apuseni Mountains, a prominent highland
292 dividing the two subsiding basins, exhibit a cluster of stable and slightly uplifted motion vectors. Plotted vectors

293 range between -2 and +2 mm/yr, with an uncertainty of 1.0 mm/yr (Table S3 of the SM). This is a general feature
294 for most stations in Europe.

295 5.3 GPS-estimated strain rates

296 We estimated strain rate variation across Romania (Fig. 5) from the regularized horizontal velocity vector field,
297 and the distribution of maximum shear strain rate and dilatation (Figs. 6 a, b). The dilatation rate quantifies the
298 extent to which the Earth's crust is either expanding or contracting. It is derived by combining the principal strain
299 rates, with positive values indicating extension and negative values indicating contraction. High positive dilatation
300 values indicate regions experiencing extension, while negative values suggest compression, as seen in processes
301 such as thrust faulting. On the other hand, the maximum shear strain rate measures the degree of shear deformation
302 within the crust, without affecting its overall volume. This is determined by calculating the difference between
303 the principal strain rates. Elevated shear strain rates are associated with regions undergoing significant shear
304 deformation, such as strike-slip fault zones, while lower values typically occur in areas experiencing
305 predominantly extensional or compressional deformation.

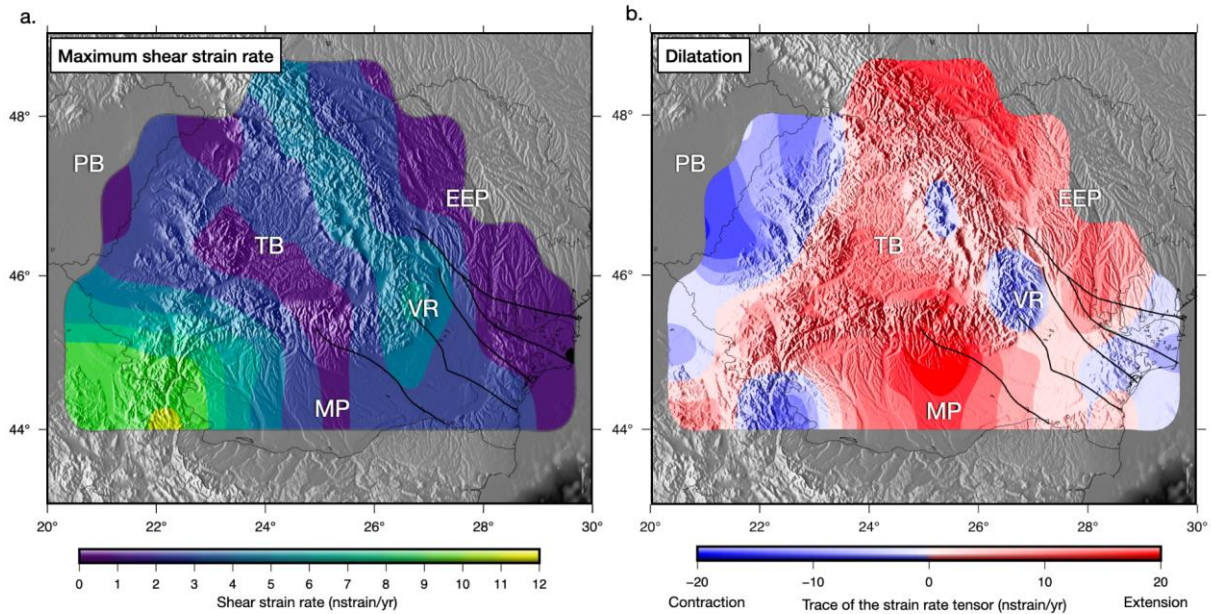


306
307 **Figure 5: Map showing the principal axes of strain rates determined from the regularized GPS horizontal**
308 **velocity vector field from this study and mechanisms of earthquakes with Mw > 3.5 from the REFMC**
309 **catalogue (Radulian et al., 2019).**

310 The distribution of strain rates is quite complex (Fig. 5 and Table S4, SM), which is expected given the region's
311 complicated tectonic framework, with multiple blocks of diverse strengths converging to form a sinuous orogenic

312 track. The highest strain rates were estimated in the southwest, at the border between Romania and Serbia. This
313 region also experiences the highest shear strain rate (Fig. 6a).

314 Dilatation patterns estimated from the strain tensor show a transition from compression in the PB to extension in
315 the intra-orogenic TB. The South Carpathians and the surrounding foreland regions, including the MP and the
316 EEP, are predominantly characterized by extension (Fig. 6b). However, localized areas of compression are
317 observed in the Eastern and South-East Carpathians, particularly in the Vrancea Zone.

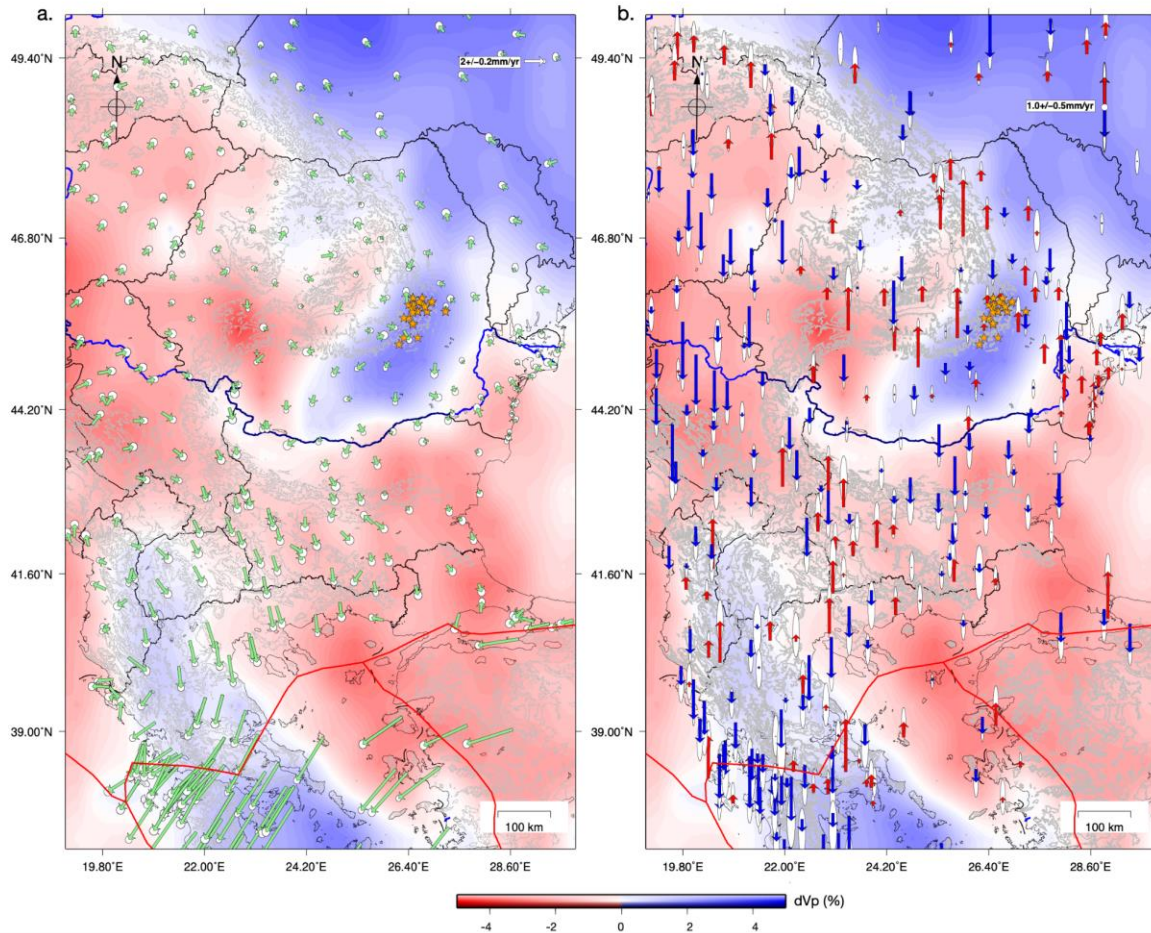


318
319 **Figure 6: Maps showing (a) maximum shear strain rate and (b) dilatational strain rate (both in**
320 **nanostrain/year), derived from the regularized GPS velocity field in Romania (Table S2, SM). The**
321 **maximum shear strain rate illustrates the intensity and direction of lateral crustal deformation, while the**
322 **dilatational strain rate is the trace of the strain rate tensor (volumetric rate of change) and indicates regions**
323 **of extension (red-positive) and compression (blue-negative). Major faults are shown as thick black lines.**
324 **Acronyms are described in the caption of Figure 1.**

325 6. Discussion

326 6.1 Regional tectonic context

327 To put our results in a broader context, we plot them against previous GPS-derived velocity vectors (Serpeloni et
328 al., 2022; Piña-Valdés et al., 2022) in Figure 7. While there is some overlap with the Romanian networks, the
329 differences between datasets are minor. To reduce clutter in the figures and minimize the impact of large tectonic
330 motions in the south, we excluded stations with an absolute horizontal velocity exceeding 7 mm/yr, as shown in
331 Figure 7a, horizontal and 7b, vertical, with the UU-07 seismic tomography model of Amaru et al. (2007), updated
332 based on Wortel and Spakman (2000), at 200 km depth, serving as background.



333

334 **Figure 7: Regional horizontal (a) and vertical crustal motions (b) from this study, Serpeloni et al. (2022), and Piña-**
 335 **Valdés et al. (2022). The horizontal vector field was scaled for visibility. The background colours show Vp seismic**
 336 **velocity anomalies at 200 km depth from the UU-P07 seismic model of Amaru et al. (2007). Red lines mark the active**
 337 **plate boundaries between Eurasia, Anatolia, and Aegean plates in the south. Orange stars mark earthquakes Mw > 6**
 338 **from the Vrancea Zone (Radulian et al., 2019).**

339 In the regional plate tectonic context, the observed velocity field highlights the complex interactions between
 340 major tectonic plates and blocks that converged in this geodynamically complex region. Seismic tomography
 341 shows the high velocity thick cratonic lithosphere to the north-east which is supposed to be tectonically stable,
 342 the Vrancea Slab as an elongated high velocity block sinking beneath the Carpathians, and the Adria and the
 343 Hellenic slabs subducting beneath the Balkan Peninsula (Fig. 7). To the south, crustal motion velocities increase
 344 significantly (Fig. 7), reflecting the rapid motion of the Hellenic subduction system as the African Plate subducts
 345 beneath the Eurasian Plate, driving southeastward deformation in Greece. Eastward, the Anatolian Plate is moving
 346 westward due to tectonic escape caused by the northward collision of the Arabian Plate with Eurasia. This
 347 westward motion is a dominant feature of the eastern Mediterranean and plays a key role in accommodating the
 348 overall regional deformation.

349 To the west, the Pannonian Basin, a hyper-extended lithosphere back-arc basin, shows relatively low horizontal
 350 deformation rates, suggesting it is currently tectonically stable, with mirror positive inversion of its eastern margin.
 351 However, the influence of the Adriatic Plate, a promontory of the African Plate, is meaningful. The Adria Plate,
 352 subducting eastwards (Fig. 7), exerts a northeastward push on the Carpathian-Pannonian system, contributing to
 353 compressional forces and tectonic inversion along the basin (Bada et al, 2007). These larger-scale processes

354 interact with the local tectonic architecture, such as the Vrancea Slab and associated seismicity (orange stars in
355 Fig. 7), resulting in a complex and heterogeneous deformation regime that bridges the stable cratonic lithosphere
356 and the active subduction-driven tectonics to the south and south-west.

357 **6.2 Correlation with earthquake mechanisms and stress indicators**

358 The GPS-derived strain rate field across Romania is characterized by a broadly distributed, long-wavelength
359 deformation pattern. At the regional scale, the field is dominated by N-S extension across much of the foreland
360 and the Carpathian chain, transitioning to localized E-W compression in the southwestern and eastern sectors (Fig.
361 6). While the GPS data provides a smooth representation of the velocity field, the discrete crustal deformation
362 captured by earthquake focal mechanisms (Fig. 5) and stress indicators from the World Stress Map (WSM2016,
363 Heidbach et al., 2007, Fig. 8) or from focal mechanisms inversion (Petrescu et al., 2021) offers a higher-resolution,
364 albeit more heterogeneous, view of how this regional strain is partitioned along inherited structures. This inherent
365 difference in spatial "wavelength" between geodetic and seismic data is essential for interpreting the transition
366 from plate-scale kinematics to fault-specific failure.

367 Despite these scale differences, we observe some spatial correlations between the strain rate and seismic regimes.
368 In the compressive domains, the negative dilatation rates observed in the Vrancea one and the Eastern Carpathians
369 (Fig. 6b) align with clusters of thrust-faulting stress indicators (Fig. 8) and reverse-faulting mechanisms (Fig. 5),
370 confirming localized crustal shortening and compression at the bend zone. Conversely, the extensional signals
371 identified in the foreland and South Carpathians are corroborated by recent normal-faulting earthquake swarms,
372 such as those occurring near the SFG (Fig. 5 and Craiu et al., 2017) and recent intense seismic sequences in the
373 South Carpathians (Radulian et al., 2023; Borleanu et al., 2024). In areas characterized by high shear strain (Fig.
374 6a), specifically the southwestern Carpathians, the prevalence of strike-slip and oblique-slip focal mechanisms
375 (Fig. 5) reflects a complex regime of strain partitioning along major fault systems. This alignment across multiple
376 independent datasets, GPS, focal mechanisms, and stress indicators, supports the reliability of the derived strain
377 field.

378

379

380

381

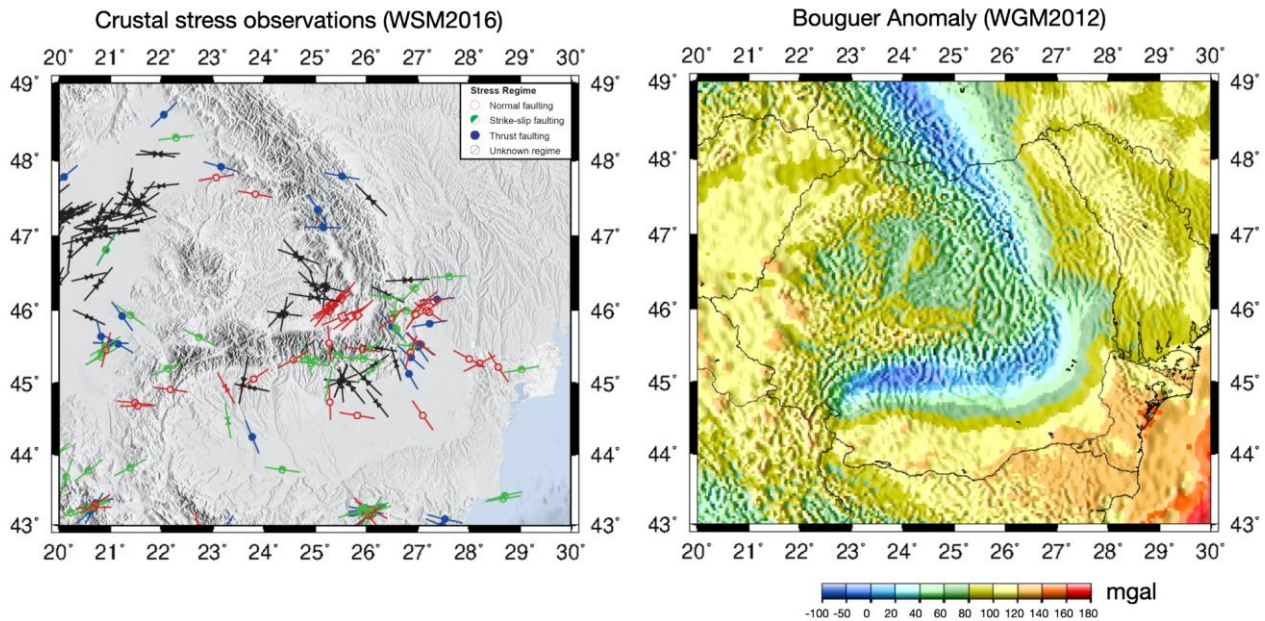
382

383

384

385

386



387 **Figure 8: Left: Crustal stress observations compiled from focal mechanisms, borehole breakouts, and other geological**
 388 **indicators, from the World Stress Map (Heidbach et al., 2018). Colours indicate the most likely stress regime. Right:**
 389 **Bouguer gravity anomalies from the World Gravity Map (WGM2012) maintained by the Bureau Gravimétrique**
 390 **International (Bonvalot et al., 2012).**

391 In regions like the Moesian Platform, the relationship between geodetic strain and seismic indicators is more
 392 nuanced. This variability in focal mechanisms, especially among smaller-magnitude events (M_w 3-4), likely
 393 reflecting the activation of secondary, oblique faults accommodating local adjustments within the regional stress
 394 framework. This complex pattern (Fig. 5) is particularly evident near large-offset faults where differing
 395 rheological properties of crustal blocks that make up the MP (Maţenco et al., 2003; Petrescu et al., 2019) and the
 396 influence of pre-existing lithospheric heterogeneities (e.g., Bertotti et al., 2003; Tărăpoancă et al., 2004) lead to
 397 pronounced strain partitioning. While the smooth GPS field is not intended to resolve every local pocket of shear
 398 or compression, the broad agreement between the primary strain axes and the dominant earthquake regimes
 399 suggests that the geodetic model reflects the regional-scale deformation patterns characterizing the Romanian
 400 crust.

401 6.3 Interactions between slab dynamics and surface uplift

402 Our results indicate a clear uplift trend in the foredeep basin area, supporting a typical post-collisional rebound
 403 and uplift behavior, as observed in many other orogenic systems. These observations differ from previous
 404 temporary GPS models (van der Hoeven et al., 2005) and lower resolution geological datasets (Merten et al., 2005,
 405 2010), which suggested that subsidence dominated the evolution of the region as a typical response to slab
 406 subduction and retreat (Tărăpoancă et al., 2004). This represents a notable change from earlier interpretations,
 407 which tended to highlight uplift in the Dobrogea forebulge while assuming subsidence further towards the
 408 Carpathian Orogen. This is also in line with some historical long-term repeated leveling methods (e.g., Popescu
 409 and Lazarescu, 1987; Joo, 1987) and is further supported by recent InSAR analyses (Poncos et al., 2022). While
 410 the continued uplift in Dobrogea is confirmed, the GPS data suggest that this uplift extends into the foredeep,
 411 highlighting the presence of vertical motions in the foredeep basin that are not solely driven by active subduction
 412 dynamics.

413 The discrepancy may reflect either a shift in the tectonic regime over time or methodological limitations in
414 capturing ongoing geodynamic processes. The observed uplift may be associated with a partial decoupling
415 between the subducting lower lithosphere and the overlying crust (Petrescu et al., 2021), allowing stress relaxation
416 and isostatic rebound of the upper crust in the foreland. This scenario is consistent with the distribution of
417 intermediate-depth seismicity and the focal mechanism patterns observed in the Vrancea Zone. In addition,
418 Mitrofan et al. (2014) suggested a partial transmission of deformation from the slab to the crust, further supporting
419 the idea of vertical stress transfer from the mantle to the surface.

420 While the continued uplift in Dobrogea is confirmed, the GPS data suggest that this uplift extends into the
421 foredeep, highlighting the presence of vertical motions in the foredeep basin that are not solely driven by active
422 subduction dynamics. Instead, the observed uplift in both regions may be linked to slab break-off, a late-stage
423 process in the subduction and continental collision cycle (Andrews and Billen, 2009). As mentioned before, the
424 Dobrogea uplifted area at the transition to the Black Sea Basin is parallel to the SE Carpathians, again suggesting
425 the interplay between collisional processes affecting the Orogen and the flexural response of the lower plate, with
426 the forebulge outward migration (from the orogen) accompanied by coeval uplift and erosion.

427 Seismic imaging suggests that the Vrancea Slab has partially torn and rotated at ~150 km depth (Martin et al.,
428 2006), leaving a deeper slab segment (200-310 km) still weakly attached (Heidbach et al., 2007). If break-off
429 continues to be active (Müller et al., 2010), asthenospheric upwelling through the torn slab segment (Petrescu et
430 al., 2023) may be dynamically supporting present-day uplift in both the SE Carpathians and foredeep. Numerical
431 simulations of subduction-collision systems with spontaneous slab break-off (Duretz et al., 2011) predict post-
432 break-off uplift rates of 0.1-0.8 km/Myr (0.1-0.8 mm/yr), which closely match our observed uplift. Additionally,
433 an increase in slab dip may promote low-wavelength lithospheric folding following continental collision (e.g.,
434 Cloetingh et al., 2004; Mařenco et al., 2007), contributing further to the uplift observed in both the SE Carpathians
435 and the foredeep.

436 Our results also reveal a significant uplift in the East Carpathians (Fig. 4), not just the SE Carpathians, raising the
437 question of whether past slab break-off there (Nemcok et al. 1998) could still be influencing present-day vertical
438 motions. Geodynamic reconstructions suggest that the subducted passive margin of the East European Platform
439 progressively broke off from north to south along the East Carpathians (Sperner et al., 1996), culminating in the
440 currently detaching Vrancea Slab (Sperner et al., 2001; Koulakov et al., 2010; Lorincz and Houseman, 2010).
441 While the initial isostatic response to slab break-off is expected to occur within a few million years (Duretz et al.,
442 2011) or up to 7 million years after convergence stops (Andrews and Billen, 2009), prolonged effects such as
443 mantle flow, residual buoyancy, and lower-crustal flow could be sustaining regional uplift. This interpretation is
444 further supported by Bouguer gravity anomalies (Fig. 8), which show relatively positive values (0–40 mGal) over
445 the mountain belt, suggesting the presence of denser material at depth or incomplete isostatic compensation. The
446 north-to-south younging of post-collisional volcanism (Seghedi et al., 2004) suggests that slab detachment
447 propagated southward over time, with the East Carpathians experiencing earlier break-off than the SE Carpathians.
448 If asthenospheric upwelling and lithospheric weakening occurred during that time, they could have led to
449 prolonged crustal adjustments that continue to manifest as uplift today.

450 In addition to the SE and East Carpathians, we also identify localized uplift in the South Carpathians. This region
451 marks the collision between the Dacia Block and the Moesian Platform, where oblique thrusting over the thick
452 Moesian lithosphere (Maţenco et al., 1997) may be inducing flexural or isostatic responses (Bertotti et al., 2003).
453 Bouguer gravity anomalies in this area transition from strongly negative values (~ -100 mGal) near the foredeep
454 in the south to over $+100$ mGal at the contact with the Transylvanian Basin (Fig. 8), indicating a shift from thick,
455 low-density crust to denser material in the north. This pattern suggests differential isostatic compensation, where
456 northward crustal thinning leads to less mass deficit and reduced buoyancy, potentially causing flexural uplift.
457 This contrast could drive vertical displacements, as observed. Alternatively, deeper mantle processes, such as
458 residual slab dynamics or lithospheric-scale deformation associated with orogenic curvature, may also influence
459 the observed uplift.

460 **7. Conclusions**

461 This study integrates the most stable and longest GPS data records from the Carpathian region of Romania over
462 a period of 20 years. Our results provide a substantial improvement in spatial coverage and resolution of vertical
463 and horizontal crustal motions in a tectonically complex region sitting at the transition between dynamically active
464 subduction systems and the stable East European Platform, with additional influences exerted by a descending
465 slab.

466 We observe pronounced horizontal southward motion in the Moesian Platform, minimal motion in the
467 Transylvanian Basin and East Carpathians, and a slight north-west motion of the Eastern European Platform, in a
468 Eurasian reference frame. The relative motions between these regions generate a dominantly extensional strain
469 field with localized zones of compression and shear, broadly consistent with stress regimes inverted from
470 earthquake clusters, although individual events capture more localized deformation heterogeneity.

471 Earlier studies in the region relied on campaign-style GPS observations. In contrast, our dataset includes cGPS
472 data from 130 stations spanning more than 20 years, providing improved spatial density and temporal resolution.
473 Our extended and more reliable data also reveal uplift in the foredeep of the SE Carpathians, challenging a
474 previously held view that this area is solely subsiding based on temporary GPS station data. This insight provides
475 a new perspective on the region's slab dynamics, which may be influenced by slab break-off and the fragmented
476 nature of the foreland, with its blocks of varying rheological strength. These differential vertical motions are
477 accommodated by seismically active faults on a crustal scale.

478 Overall, this study significantly advances our understanding of the tectonic processes that shape regions at the
479 intersection of active subduction/collision zones and stable continental platforms. It provides key constraints on
480 the interplay between slab dynamics, surface plate kinematics, and the resulting crustal deformation, an essential
481 step toward improving seismic hazard assessment.

482 **Code availability**

483 The GipsyX software is licensed to the Department of Geophysics of the University of Bucharest (UNIBUC). We
484 were allowed to use this software in an ongoing collaboration with UNIBUC. The strain rate estimation code

485 STRAINTOOL (Anastasiou et al., 2021) is available at <https://github.com/DSOlab/StrainTool> (accessed in
486 January 2025). Most figures were made using the open-source GMT software (Wessel et al., 2013).

487 **Data availability**

488 The RINEX-format GNSS data (sampled at 30s intervals) analysed in this study are only available from the NIEP
489 (National Institute of Earth Physics) network online at <http://gps.infp.ro/#/>. The rest of the data can be made
490 available from the organisations responsible with their maintenance upon reasonable request and data sharing
491 agreements. All individual velocity solutions and strain rate estimates from this study are provided in the SM.

492 **Author contributions**

493 **AM:** Conceptualization, Methodology, Data Curation, Formal analysis, Investigation, Writing - Original Draft,
494 Visualization **LP:** Formal analysis, Writing - Original Draft, Visualization **BA:** Software, Data Curation, Formal
495 analysis, Visualization, Writing - Review & Editing, Supervision **FB:** Writing - Review & Editing **EN:** Writing -
496 Review & Editing, Managed the NIEP GNSS network technically **IM:** Writing - Review & Editing

497 **Competing interests**

498 The authors declare that they have no conflict of interest.

499 **Acknowledgments**

500 We acknowledge the Netherlands Research Centre for Integrated Solid Earth Science (ISES) for the initial
501 establishment in 2001 of seven cGPS stations in Romania dedicated to long term geodetic and geophysical
502 research in the region. This early enterprise comprised a collaborative effort of the University of Bucharest (V.
503 Mocanu), the National Institute for Earth Physics (L. Munteanu), the Delft University of Technology (B.A.C.
504 Ambrosius) and the Utrecht University (W. Spakman). We thank the National Research and Development Institute
505 for Marine Geology and Geo-Ecology, National Center for Monitoring and Alarm to Natural Marine Hazards –
506 Euxinus, as well as the National Agency for Cadaster and Land Registration, and the TopGeocart company for
507 providing access to their data. The authors thank Dr. Stefan Leinen, an anonymous reviewer, and the editors for
508 their constructive comments on the original manuscript.

509 **Financial support**

510 This research was carried out within the NUCLEU project, SOL4RISC Program which is supported by the
511 Ministry of Education and Research, project nr. PN23360201. This work was also supported by the European
512 Union (Next Generation EU instrument) through the National Recovery and Resilience Plan, "PNRR-III-C9-2022
513 – I5 Establishment and operationalization of Competence Centers" competition, "Competence Center for Climate
514 Change Digital Twin for Earth forecasts and societal redressment: DTEClimate" project, contract
515 no.760008/30.12.2022, code 7/16.11.2022. Additional support was provided through the CRESCENTO Project

516 (no. 346/390022/08.09.2021, SMIS no. 127463) and the GEOMONITOR Project (contract no. 28Sol(T28)/2025),
517 funded by the Ministry of Education and Research through UEFISCDI within PNCDI IV.

518 **References**

519 Altamimi, Z., Métivier, L., Rebischung, P., Rouby, H., and Collilieux, X.: ITRF2014 plate motion model,
520 *Geophys. J. Int.*, 209, 1906–1912, <https://doi.org/10.1093/gji/ggx136>, 2017.

521 Anastasiou D.G., Papanikolaou X., Ganas A., and Paradissis D.: StrainTool: A software package to estimate strain
522 tensor parameters. Zenodo; Version 1.1, <https://doi.org/10.5281/zenodo.5501234>, 2021.

523 Amaru, M. L.: Global travel time tomography with 3-D reference models, PhD thesis, Utrecht Univ., Utrecht,
524 Netherlands, 2007.

525 Andrews, E. R. and Billen, M. I.: Rheologic controls on the dynamics of slab detachment, *Tectonophysics*, 464,
526 60-69, <https://doi.org/10.1016/j.tecto.2007.09.004>, 2009.

527 Bada, G., Horváth, F., Dövényi, P., Szafián, P., Windhoffer, G. and Cloetingh, S.: Present-day stress field and
528 tectonic inversion in the Pannonian basin, *Global Planet. Change*, 58, 165-180,
529 <https://doi.org/10.1016/j.gloplacha.2007.01.007>, 2007.

530 Balla, Z.: Palaeotectonic reconstruction of the central Alpine-Mediterranean belt for the Neogene,
531 *Tectonophysics*, 127, 213-243, [https://doi.org/10.1016/0040-1951\(86\)90062-4](https://doi.org/10.1016/0040-1951(86)90062-4), 1986.

532 Bertiger, W., Bar-Sever, Y., Dorsey, A., Haines, B., Harvey, N., Hemberger, D., Heflin, M., Lu, W., Miller, M.,
533 Moore, A.W., Murphy, D., Ries, P., Romans, L., Sibois, A., Sibthorpe, A., Szilagyi, B., Vallisneri, M., and Willis,
534 P.: GipsyX/RTGx, a new tool set for space geodetic operations and research, *Advances in Space Research*, 66,
535 469–489, <https://doi.org/10.1016/j.asr.2020.04.015>, 2020.

536 Bertotti, G., Maţenco, L. and Cloetingh, S. A. P. L.: Vertical movements in and around the south-east Carpathian
537 foredeep: lithospheric memory and stress field control. *Terra Nova*, 15, 299-305, 2003.

538 Beşuţiu, L., Manea, V., Pomeran, M.: Vrancea seismic zone as an unstable triple junction: new evidence from
539 observations and numerical modelling. In: 9th Congress of the Balkan Geophys. Soc, vol. 2017. European
540 Association of Geoscientists & Engineers, 1-5, <https://doi.org/10.3997/2214-4609.201702541>, 2017.

541 Blewitt, G., Lavallée, D., Clarke, P., and Nurutdinov, K.: A new global mode of Earth deformation: Seasonal
542 cycle detected, *Science*, 294, 2.342-2.345, <https://doi.org/10.1126/science.106532001>, 2001.

543 Bonvalot, S., Balmino, G., Briais, A., M. Kuhn, Peyrefitte, A., Vales, Biancale, R., Gabalda, G., Moreaux, G.,
544 Reinquin, F., and Sarrailh, M.: World Gravity Map, 1:50000000 map, Eds.: BGI-CGMW-CNES-IRD, Paris, 2012.

545 Bos. M. S., and Scherneck, H., G.: Ocean tide loading provider, <http://holt.oso.chalmers.se/loading/index.html>,
546 2011.

547 Borleanu F., Petrescu L., Fojtikova L., Munteanu I., Silvennoinen H., Placinta A.O., Oros E., and Enescu B.: ML
548 5.7 Southern Carpathians earthquake sequence: Insights from seismic observations, ESC2024-S17/50-808,
549 https://www.erasmus.gr/UsersFiles/microsite1277/Documents/ESC2024_Abstract_Book.pdf, 2024.

550 Cloetingh, S. A. P. L., Burov, E., Matenco, L., Toussaint, G., Bertotti, G., Andriessen, P. A. M., Wortel, M. J. R.
551 and Spakman, W.: Thermo-mechanical controls on the mode of continental collision in the SE Carpathians
552 (Romania), *Earth Planet. Sc. Lett.*, 218, 57-76, 2004.

553 Cloetingh, S., Bada, G., Maţenco, L., Lankreijer, A., Horváth, F. and Dinu, C.: Modes of basin (de) formation,
554 lithospheric strength and vertical motions in the Pannonian-Carpathian system: inferences from thermo-
555 mechanical modelling, *Geo. Soc. Mem.*, 32, 207-221, DOI: 10.1144/GSL.MEM.2006.032.01.12, 2006.

556 Cornea, I., Dragoescu, I., Popescu, M. N., and Visarion, M.: Monography of recent vertical crustal movements in
557 the S. R. of Romania (in Romanian), Preprint Central Inst. of Phys., 100, 1978.

- 558 Cornea, I., and Popescu, M. N.: The Vrancea Earthquake of March 4. 1977 and the Recent crustal vertical
559 movements in Romania. In Cornea & Radu (Editors): Seismological Research of March 4. 1977 Earthquake (in
560 Romanian), Preprint Central Inst. of Phys., 559 - 568, 1979a.
- 561 Cornea, I., Dragoescu, I., Popescu, M. N., and Visarion, M.: Map of recent vertical crustal movements of the
562 territory of S. R. of Romania (in Romanian), St. Cerc. Geol., Geofiz., Geogr., Geofizica, 17, 3-20, 1979b.
- 563 Craiu, A., Craiu, M., Diaconescu, M. and Marmureanu, A.: 2013 Seismic swarm recorded in Galati area,
564 Romania: focal mechanism solutions, Acta Geod. Geophys., 52, 53-67, 2017.
- 565 Csontos, L., and Vörös, A.: Mesozoic plate tectonic reconstruction of the Carpathian region, Palaeogeography,
566 Palaeoclimatology, Palaeoecology, 210, 1-56, <https://doi.org/10.1016/j.palaeo.2004.02.033>, 2004.
- 567 Dinter, G., and Schmitt, G.: Three Dimensional Plate Kinematics in Romania, Nat. Hazards, 23, 389–406,
568 <https://doi.org/10.1023/A:1011116615142>, 2001.
- 569 Duretz, T., Gerya, T. V. and May, D. A.: Numerical modelling of spontaneous slab breakoff and subsequent
570 topographic response, Tectonophysics, 502, 244-256, <https://doi.org/10.1016/j.tecto.2010.05.024>, 2011.
- 571 Enescu, B., Ghita, C., Moldovan, I.A. and Radulian, M.: Revisiting Vrancea (Romania) intermediate-depth
572 seismicity: some statistical characteristics and seismic quiescence testing. Geosciences, 13, 21,
573 <https://doi.org/10.3390/geosciences13070219>, 2023.
- 574 Heidbach, O., Ledermann, P., Kurfeß, D., Peters, G., Buchmann, T., Matenco, L., Negut, M., Sperner, B., Müller,
575 B., and Nuckelt, A.: Attached or not attached: slab dynamics beneath Vrancea, Romania, In: International
576 symposium on strong Vrancea earthquakes and risk mitigation, 4–20, 2007.
- 577 Heidbach, O., Rajabi, M., Cui, X., Fuchs, K., Müller, B., Reinecker, J., Reiter, K., Tingay, M., Wenzel, F., Xie,
578 F. and Ziegler, M.O.: The World Stress Map database release 2016: Crustal stress pattern across scales.
579 Tectonophysics, 744, 484-498, 2018.
- 580 Hippolyte, J.C.: Geodynamics of Dobrogea (Romania): new constraints on the evolution of the Tornquist–
581 Teisseyre Line, the Black Sea and the Carpathians, Tectonophysics, 357, 33-53, [https://doi.org/10.1016/S0040-1951\(02\)00361-X](https://doi.org/10.1016/S0040-1951(02)00361-X), 2002.
- 583 Ismail-Zadeh, A., Mañenco, L., Radulian, M., Cloetingh, S. and Panza, G.: Geodynamics and intermediate-depth
584 seismicity in Vrancea (the south-eastern Carpathians): current state-of-the art. Tectonophysics, 530, 50-79, DOI:
585 10.1016/j.tecto.2012.01.016, 2012.
- 586 Joó, I., Arabadžijski, D., Fűry, M., Meščerski, I. N., Mihăila, M., Mladenovski, M. M., Németh, Z., Steinberg, J.,
587 Thury, J., Vanko, J., and Wyrzykowski, T.: New investigations on recent vertical movements in the Carpatho-
588 Balkan region, J. Geodyn., 8, 99-113, [https://doi.org/10.1016/0264-3707\(87\)90028-7](https://doi.org/10.1016/0264-3707(87)90028-7), 1987.
- 589 Koulakov, I., Zaharia, B., Enescu, B., Radulian, M., Popa, M., Parolai, S. and Zschau, J.: Delamination or slab
590 detachment beneath Vrancea? New arguments from local earthquake tomography, Geochem. Geophys. Geosy.,
591 11, <https://doi.org/10.1029/2009GC002811>, 2010.
- 592 Krézsek, C., Lăpădat, A., Mañenco, L., Arnberger, K., Barbu, V., and Olaru, R.: Strain partitioning at orogenic
593 contacts during rotation, strike–slip and oblique convergence: Paleogene–Early Miocene evolution of the contact
594 between the South Carpathians and Moesia, Global Planet. Change, 103, 63–81, <https://doi.org/10.1016/j.gloplacha.2012.11.009>, 2013.
- 596 Lorinczi, P., and Houseman, G.: Lithospheric gravitational instability beneath the Southeast Carpathians,
597 Tectonophysics, 474, 322–336, <https://doi.org/10.1016/j.tecto.2008.05.024>, 2009.
- 598 Mañenco L, Zoetemeijer R, Cloetingh S, and Dinu C.: Lateral variations in mechanical properties of the Romanian
599 external Carpathians: inferences of flexure and gravity modelling. Tectonophysics, 282,147-166, 1997.
- 600 Mañenco, L., and Bertotti, G.: Tertiary tectonic evolution of the external East Carpathians (Romania),
601 Tectonophysics, 316, 255–286, [https://doi.org/10.1016/S0040-1951\(99\)00261-9](https://doi.org/10.1016/S0040-1951(99)00261-9), 2000.
- 602 Mañenco L, Bertotti G, Cloetingh S, and Dinu C; Subsidence analysis and tectonic evolution of the external
603 Carpathian-Moesian platform region during Neogene times. Sed Geol, 156(14), 71-94, 2003.
- 604 Mañenco, L., Bertotti, G., Leever, K., Cloetingh, S.A.P.L., Schmid, S.M., Tărăpoancă, M., and Dinu, C.: Large-
605 scale deformation in a locked collisional boundary: Interplay between subsidence and uplift, intraplate stress, and

- 606 inherited lithospheric structure in the late stage of the SE Carpathians evolution, *Tectonics*, 26,
607 <https://doi.org/10.1029/2006TC001951>, 2007.
- 608 Merten, S., Andriessen, P. A. M., Juez-Larré, J., Bertotti, G. V., and Dunai, T. J.: Dating the exhumation of the
609 Romanian Carpathians: first results from apatite (U-Th)/He thermochronology, *Abstract from Geophysical*
610 *Research Abstracts*, 7, 08138, [https://meetings.copernicus.org/www.cosis.net/abstracts/EGU05/08138/EGU05-J-](https://meetings.copernicus.org/www.cosis.net/abstracts/EGU05/08138/EGU05-J-08138.pdf)
611 [08138.pdf](https://meetings.copernicus.org/www.cosis.net/abstracts/EGU05/08138/EGU05-J-08138.pdf), 2005.
- 612 Merten S., Matenco L., Foeken J. P. T., Stuart F. M., and Andriessen P. A. M.: From nappe stacking to out-of-
613 sequence postcollisional deformations: Cretaceous to Quaternary exhumation history of the SE Carpathians
614 assessed by low-temperature thermochronology, *Tectonics*, 29, <https://doi.org/10.1029/2009TC002550>, 2010.
- 615 Müller, B., Heidbach, O., Negut, M., Sperner, B. and Buchmann, T.: Attached or not attached—evidence from
616 crustal stress observations for a weak coupling of the Vrancea slab in Romania, *Tectonophysics*, 482, 139-149,
617 <https://doi.org/10.1016/j.tecto.2009.08.022>, 2010.
- 618 Muntean, A., Mocanu, V., Ambrosius, B.: A GPS study of land subsidence in the Petrosani (Romania) coal
619 mining area. *Nat. Hazards*, 80, 797–810, DOI:10.1007/s11069-015-1997-y, 2016.
- 620 Necea, D., Fielitz, W., and Matenco, L.: Late Pliocene–Quaternary tectonics in the frontal part of the SE
621 Carpathians: Insights from tectonic geomorphology, *Tectonophysics*, 410, 137-156,
622 <https://doi.org/10.1016/j.tecto.2005.05.047>, 2005.
- 623 Necea D., Fielitz W., Kadereit A., P.A.M. Andriessen P.A.M., and Dinu C.: Middle Pleistocene to Holocene
624 fluvial terrace development and uplift-driven valley incision in the SE Carpathians, Romania, *Tectonophysics*,
625 602, 332-354, <https://doi.org/10.1016/j.tecto.2013.02.039>, 2013.
- 626 Necea, D., Juez-Larré, J., Matenco, L., Andriessen, P. A.M., and Dinu C.: Foreland migration of orogenic
627 exhumation during nappe stacking: Inferences from a high-resolution thermochronological profile over the
628 Southeast Carpathians, *Global Planet. Change*, 200, 103457, <https://doi.org/10.1016/j.gloplacha.2021.103457>,
629 2021.
- 630 Nemcok, M., Pospisil, L., Lexa, J., and Donelick, R.A.: Tertiary subduction and slab break-off model of the
631 Carpathian–Pannonian region, *Tectonophysics*, 295, 307-340, [https://doi.org/10.1016/S0040-1951\(98\)00092-4](https://doi.org/10.1016/S0040-1951(98)00092-4),
632 1998.
- 633 Petrescu, L., Stuart, G., Tataru, D., and Grecu, B.: Crustal structure of the Carpathian Orogen in Romania from
634 receiver functions and ambient noise tomography: how craton collision, subduction and detachment affect the
635 crust. *Geophys. J. Int.*, 218, 163-178, <https://doi.org/10.1093/gji/ggz140>, 2019.
- 636 Petrescu, L., Borleanu, F., Radulian, M., Ismail-Zadeh, A., and Mațenco, L.: Tectonic regimes and stress patterns
637 in the Vrancea Seismic Zone: Insights into intermediate-depth earthquake nests in locked collisional settings,
638 *Tectonophysics*, 799, 228688, <https://doi.org/10.1016/j.tecto.2020.228688>, 2021.
- 639 Petrescu, L., Mihai, A. and Borleanu, F.: Slab tear and rotation imaged with core-refracted shear wave anisotropy.,
640 *J. Geodyn.*, 157, 101985, <https://doi.org/10.1016/j.jog.2023.101985>, 2023.
- 641 Petrescu, L. and Enescu, B.: Seismicity of a relic slab: space–time cluster analysis in the Vrancea Seismic Zone.
642 *Earth, Planets and Space*, 77, 6., <https://doi.org/10.1186/s40623-025-02136-6>, 2025.
- 643 Piña-Valdés, J., Socquet, A., Beauval, C., Doin, M.-P., D’Agostino, N., and Shen, Z.-K.: 3D GNSS velocity field
644 sheds light on the deformation mechanisms in Europe: Effects of the vertical crustal motion on the distribution of
645 seismicity, *J. Geophys. Res.-Sol. Ea.*, 127, e2021JB023451, <https://doi.org/10.1029/2021JB023451>, 2022.
- 646 Poncos, V., Stanciu, I., Teleaga, D., Mațenco, L., Bozsó, I., Szakács, A., Birtas, D., Toma, S.A., Stanica, A.,
647 and Radulescu, V.: An Integrated Platform for Ground-Motion Mapping, Local to Regional Scale; Examples
648 from SE Europe. *Remote Sensing*, 14, 1046, [10.3390/rs14041046](https://doi.org/10.3390/rs14041046), 2022.
- 649 Popa, M., Chircea, A., Dinescu, R., Neagoe, C., Grecu, B., and Borleanu, F.: Romanian earthquake catalogue
650 (ROMPLUS). *Mendeley Data*, 2, 2022.
- 651 Popescu, M. N., and Drăgoescu, I.: Maps of recent vertical crustal movements in Romania: Similarities and
652 differences, *J. Geodyn.*, 8, 123-136, [https://doi.org/10.1016/0264-3707\(87\)90030-5](https://doi.org/10.1016/0264-3707(87)90030-5), 1987.

- 653 Radulian, M., Bălă, A., Ardeleanu, L., Toma-Dănilă, D., Petrescu, L., and Popescu, E.: Revised catalogue of
654 earthquake mechanisms for the events occurred in Romania until the end of twentieth century: REFMC, Acta
655 Geod. Geophys., 54, 3-18, <https://doi.org/10.1007/s40328-018-0243-y>, 2019.
- 656 Radulian, M., Popa, M., Dinescu, R., and Bala, A.: Location improvements for the twin crustal earthquakes
657 recorded in February 2023 in Gorj County, Romania. International Multidisciplinary Scientific GeoConference:
658 SGEM, 23(1.1), 57-64, 2023.
- 659 Ren, Y., Stuart, G., Houseman, G., Dando, B., Ionescu, C., Hegedüs, E., Radovanović, S., and Shen, Y.: Upper
660 mantle structures beneath the Carpathian–Pannonian region: Implications for the geodynamics of continental
661 collision, Earth Planet. Sc. Lett., 349, 139–152. <https://doi.org/10.1016/j.epsl.2012.06.037>, 2012.
- 662 re3data.org: VMF Data Server; editing status 2024-05-15; re3data.org - Registry of Research Data Repositories,
663 <https://doi.org/10.17616/R3RD2H>
- 664 Sanders, C., Andriessen, P., and Cloetingh, S.: Life cycle of the East Carpathian orogen: erosion history of a
665 doubly vergent critical wedge assessed by fission track thermochronology, J. Geophys. Res., 104, 29095–29112,
666 <https://doi.org/10.1029/1998JB900046>, 1999.
- 667 Schmid, S.M., Fügenschuh, B., Kounov, A., Maţenco, L., Nievergelt, P., Oberhänsli, R., Pleuger, J., Schefer, S.,
668 Schuster, R., Tomljenović, B., and Ustaszewski, K.: Tectonic units of the Alpine collision zone between Eastern
669 Alps and western Turkey, Gondwana Res., 78, 308-374, <https://doi.org/10.1016/j.gr.2019.07.005>, 2020.
- 670 Seghedi, A., Lang, B. and Heimann, A.: The deformational history of North Dobrogean Hercynian basement as
671 reflected in new $^{39}\text{Ar}/^{40}\text{Ar}$ determinations, Romanian Journal of Tectonics and Regional Geology, 77, 64-65,
672 <https://doi.org/10.3906/YER-1101-20>, 1999.
- 673 Seghedi, I., Downes, H., Vaselli, O., Szakács, A., Balogh, K. and Pécskay, Z.: Post-collisional Tertiary–
674 Quaternary mafic alkalic magmatism in the Carpathian–Pannonian region: a review, Tectonophysics, 393, 43-62,
675 <https://doi.org/10.1016/j.tecto.2004.07.051>, 2004.
- 676 Serpelloni, E., Cavaliere, A., Martelli, L., Pintori, F., Anderlini, L., Borghi, A., Randazzo, D., Bruni, S., Devoti,
677 R., Perfetti, P., and Cacciaguerra, S.: Surface Velocities and Strain-Rates in the Euro-Mediterranean Region From
678 Massive GPS Data Processing, Front. Earth Sci., 10, 907897, <https://doi.org/10.3389/feart.2022.907897>, 2022.
- 679 Shen, Z. K., Wang, M., Zeng, Y., and Wang, F.: Strain determination using spatially discrete geodetic data, Bull.
680 Seismol. Soc. Am., 105, 2117-2127, <https://doi.org/10.1785/0120140247>, 2015.
- 681 Sperner, B.: Computer programs for the kinematic analysis of brittle deformation structures and the Tertiary
682 tectonic evolution of the Western Carpathians. Tübingen Geoscientific Works (TGA) Series A. Geology,
683 Paleontology, Stratigraphy 27 (NEBIS)001536648EBI01, 1996.
- 684 Sperner, B., Lorenz, F., Bonjer, K., Hettel, S., Müller, B., and Wenzel, F: Slab break-off–abrupt cut or gradual
685 detachment? New insights from the Vrancea Region (SE Carpathians, Romania), Terra Nova, 13, 172-179,
686 <https://doi.org/10.1046/j.1365-3121.2001.00335.x>, 2001.
- 687 Tărăpoancă, M., Garcia-Castellanos, D., Bertotti, G., Matenco, L., Cloetingh, S., and Dinu, C.: Role of the 3-D
688 distributions of load and lithospheric strength in orogenic arcs: polystage subsidence in the Carpathians foredeep,
689 Earth Planet. Sc. Lett., 221, 163–180, [https://doi.org/10.1016/S0012-821X\(04\)00068-8](https://doi.org/10.1016/S0012-821X(04)00068-8), 2004.
- 690 Van der Hoeven, A., Mocanu, V., Spakman, W., Nutto, M., Nuckelt, A., Matenco, L., Munteanu, L., Marcu, C.,
691 and Ambrosius, B.: Observation of present-day tectonic motions in the Southeastern Carpathians: Results of the
692 ISES/CRC-461 GPS measurements, Earth Planet. Sc. Lett., 239, 177-
693 184, <https://doi.org/10.1016/j.epsl.2005.09.018>, 2005.
- 694 Wenzel, F., Lorenz, F., Sperner, B., and Oncescu, M. C.: Seismotectonics of the Romanian Vrancea area, Vrancea
695 Earthquakes: Tectonics, Hazard and Risk Mitigation, 15–26, Kluwer Acad., 1999.
- 696 Wessel, P., W. H. Smith, R. Scharroo, J. Luis, and F. Wobbe: Generic Mapping Tools: Improved Version
697 Released, Eos, Trans. AGU, 94, 409–410, <https://doi.org/10.1002/2013EO450001>, 2013.
- 698 Wortel, M.J.R. and Spakman, W.: Subduction and slab detachment in the Mediterranean-Carpathian region,
699 Science, 290, 1910-1917, <https://doi.org/DOI:10.1126/science290.5498.1910>, 2000.